SDSS'Rio 2010 STABILITY AND DUCTILITY OF STEEL STRUCTURES
E. Batista, P. Vellasco, L. de Lima (Eds.)
Rio de Janeiro, Brazil, September 8 - 10, 2010

PLASTIC COLLAPSE MECHANISMS IN COMPRESSED ELLIPTICAL HOLLOW SECTIONS

Aimar Insausti* and Leroy Gardner*

* Department of Civil and Environmental Engineering, Imperial College London, London SW7 2AZ
e-mails: a.insausti@imperial.ac.uk, leroy.gardner@imperial.ac.uk

Keywords: Compression; Elliptical hollow sections; Local buckling; Plastic mechanism; Steel structures.

Abstract. *The plastic collapse response of structural steel elliptical hollow section (EHS) profiles in compression is examined in this paper. As an initial step, a parametric study to identify the factors that determine which plastic mechanisms would arise has been carried out using finite element (FE) results from the current work and experimental data from the literature. Following this, an analytical model to describe the "split flip disc" plastic collapse mechanism in compressed EHS is derived. The parameters controlling the shape and size of the plastic hinges have been investigated and found to be of key importance; hence, special care has been taken in their definition. Finally, the analytically derived load–displacement curves have been compared with FE results. The comparisons have revealed good agreement, confirming the ability of the developed analytical models to predict the plastic collapse response of elliptical tubes.*

1 INTRODUCTION

Hot-finished structural steel elliptical hollow sections (EHS) have recently been introduced to the construction sector. These structural elements can offer greater structural efficiency than circular hollow sections (CHS) when subjected to bending or combined loading, or when used as columns with intermediate restraint about the weaker axis, since they posses different major and minor axis flexural properties. Despite recent investigations involving the testing, numerical modelling and development of design rules for EHS, a number of aspects of their structural response remain unexplored. In particular, the behaviour of elliptical profiles in the post ultimate region has not yet been examined.

The aim of the present work is to develop an analytical model to predict the load–deformation response of EHS under pure compression. To this end, rigid-plastic theory has been applied to EHS based on the method presented by Murray for plates [1]. As an initial step, a parametric study was carried out to identify the most common local plastic collapse mechanisms arising in EHS. The study involved finite element (FE) modelling and the analysis of existing test data [2]. Whilst a number of failure modes were identified, an inward plastic collapse mechanism of the form shown in Fig. 1 was the most prominent. An analytical description of this collapse mechanism is therefore the focus of the present study. The key parameters controlling the size and shape of the hinge lines in the plastic mechanism were carefully examined and their influence on the overall load–deformation response was assessed. Finally, comparisons between the analytical model and the results obtained from the FE models are presented.

2 LITERATURE REVIEW

The intermediate response of elliptical tubes between that of flat plates and circular shells has been previously identified in terms of elastic buckling [3]. In anticipation of an analogous scenario for plastic collapse, previous studies on rigid-plastic failure mechanisms in flat plates and circular shells are initially reviewed. For rigid-plastic mechanisms in flat plates, pioneering work was carried out by Murray [1], who introduced a number of different failure modes and derived corresponding load–deformation curves. Among the common plate-like patterns identified, the so called "flip disc" mechanism was presented in

detail. This mechanism is formed by two curved hinge lines, one of them folding outwards and the other inwards, creating a disc shape plate within the hinge lines that flips around the horizontal mid axis.

Research on compressed CHS has identified two main local plastic failure modes - the "elephant foot" and "Yoshimura" mechanisms. The elephant foot is an axisymmetrical mode with outwards deformation that creates a concertina shape in the surface, while the Yoshimura pattern includes several sequential folding lines that deform the cross-section in a non axisymetrical way. The boundaries that define the occurrence of each plastic failure mode were studied experimentally by Andrews et al. [4]. Both failure modes as well as a mixed mode were identified in the experimental work and a classification chart to predict their occurrence was developed. Later, the available experimental data on compressed CHS was expanded by Guillow et al. [5] carrying out more tests over a wider cross-section slenderness range. As a consequence, a revised classification chart was developed. For the elephant foot mode, load-displacement curves were derived by Grzebieta [6] using the plastic mechanism approach. Further experimental results on circular tubes specifically proportioned to develop axisymmetric failure modes were presented by Gupta and Velmurugan [7] while Johnson et al. [8] studied the Yoshimura type mechanism by means of tests on circular PVC tubes.

The key difference between the elements previously studied (i.e. flat plates and CHS) and elliptical hollow sections lies in the continuously varying curvature brought about by the following geometrical definition where the symbols are defined in Fig. 1.

$$\frac{z^2}{a^2}+\frac{y^2}{b^2}=1 \tag{1}$$

With the recent introduction of hot-finished EHS into the construction sector, heightened interest in the structural behaviour of elliptical profiles, as well as the need to develop design guidance, have emerged. Structural performance data have been generated on elliptical sections in compression [2, 9] and bending [10]. The result of the 25 compression tests (stub column tests) given in [2], together with numerically generated results, have been used in the present study for the development and validation of the analytical model. Based on the results of compression and bending tests [2, 10] and an analysis of the elastic buckling of EHS, a cross-section slenderness parameter was derived for the purpose of cross-section classification [11]. The slenderness parameter was based on an equivalent diameter D_e, which allowed the classification of EHS to be made on the basis of the CHS slenderness limits. For the pure compression case, $D_e = 2a^2/b$, which corresponds to the point in the section with maximum radius of curvature, 2a and 2b being the larger and smaller outer dimensions respectively of the EHS, as shown in Fig. 1. This point of the section was identified by Kempner [12] as suitable for use with the classical formula for CHS in determining elastic buckling stresses for EHS. Later, more precise expressions for determining the equivalent diameter were proposed [3, 13], and an alternative approach to EHS classification, based on an equivalent rectangular hollow section has also been investigated [9].

3 FINITE ELEMENT MODELLING

In this section, the use of FE analysis to examine the behaviour of stocky EHS under compression is described. These models have already been validated against a total of 25 compression tests in [2]. As well as being used to generate a series of load–deflection curves that will be used to validate the analytical model presented later, the FE models were used to identify the different plastic collapse mechanisms arising for different geometries, making it possible to focus the research on the more common plastic collapse modes. The FE models also provided useful information about the size and shape of the mechanism throughout the deformation process.

All models were developed using the nonlinear FE software ABAQUS. The elements designated as S4R in ABAQUS were employed throughout the modelling. The cross-sectional dimensions of the modelled elliptical sections was kept constant at 150×75 mm, while the thicknesses used were 4, 5, 6.3 and 8 mm, covering a range of cross-section slenderness values. The above thickness values are also representative of commercially available profiles and consistent with those previously studied

experimentally. The member length was fixed at 300 mm, which was sufficiently short to ensure no global buckling, and all sections were subjected to concentric compression. All models were assigned rigid-plastic material properties without strain-hardening or residual stresses to allow direct comparison with the analytical model developed herein.

Fixed boundary conditions were applied to the ends of the columns, with all degrees of freedom, other than vertical displacement at the loaded end, restrained. Initial geometric imperfections were introduced in the shape of elastic buckling modes obtained from eigenvalue analyses. Three modes were considered, in which the number of half sine waves along the stub column length was either odd or even, the imperfection was either positive or negative (positive being inwards at the mid-height of the stub column) and the imperfection was either symmetrical or asymmetrical about the mid-height. Three imperfection amplitudes were also considered: t, t/10, t/100, where t is the section thickness.

4 IDENTIFICATION OF PLASTIC MECHANISMS IN EHS

According to plastic theory, the number of possible plastic mechanisms in a thin-walled structure is unlimited; however, some plastic failure patterns are more commonly repeated when the element is loaded in a specific way. The present section discusses the trend of the elliptical profiles to follow specific failure mechanisms with reference to the FE and test results. Hence, the more common local plastic failure modes in EHS can be identified and focussed upon in the analytical study.

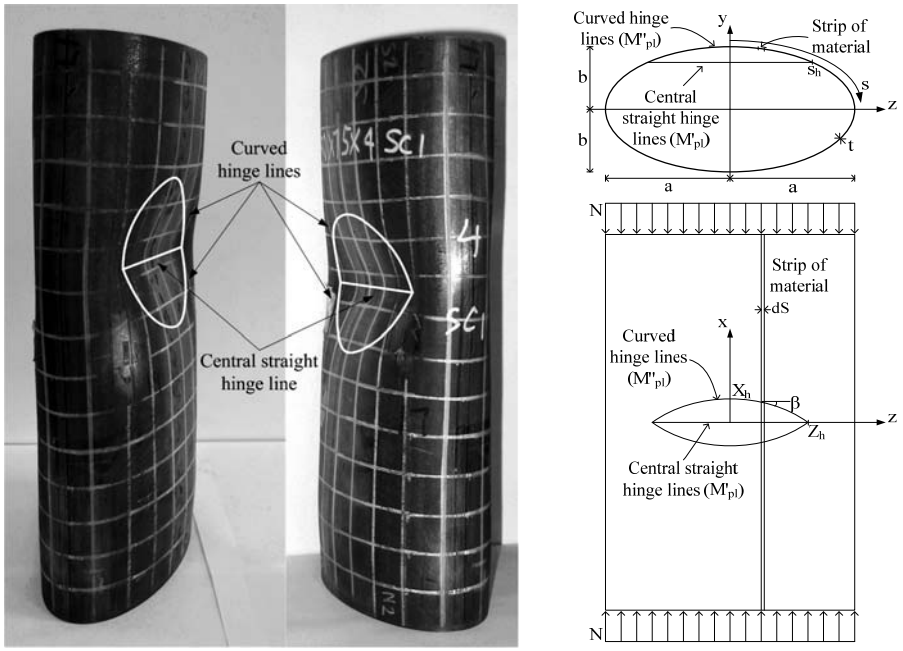

Figure 1. (a) Split flip disc failure pattern observed in tests and (b) illustration of the mechanism.

Variation of the initial geometrical imperfections described in the previous section trigger four different plastic failure patterns, two of them akin to plate-like behaviour and the other two akin to shell-like (CHS) behaviour. Within the plate failure modes, one of them is similar to the flip disc mechanism proposed by Murray [1] for flat plates, while the other is a variation of it. This variation includes an extra straight hinge line in the middle of the mechanism splitting the disc into two half parts as shown in Fig. 1. This plastic mechanism is referred to herein as the split flip disc (SFD) mechanism. The shell-like plastic

collapse mechanisms observed in the EHS are the elephant foot and the Yoshimura patterns. All four mechanisms are shown in Fig. 2.

The specific failure mode that a given EHS profile would succumb to was found to be influenced by the shape and amplitude of the initial geometric imperfection, as well as the slenderness (D_e/t, where $D_e = 2a^2/b$) of the cross-section. The FE models showed that plate-like failure modes dominate the profile's behaviour for smaller (and more practical) levels of initial imperfection, and that, overall, the split flip disc mechanism was the most common.

The experimental work presented in [2] has also been used to identify the plastic failure mechanisms in compressed EHS. The tests exhibited three of the four modes revealed in the numerical study: the flip disc, the split flip disc and the elephant foot modes. However, the elephant foot was present only in four out of 25 tests. The flip disc and the split flip disc modes appeared in the remaining 21 tests in no clear pattern; overall, the split flip disc mechanism appeared more frequently. Hence, the most commonly arising mode in both the experimental and numerical studies was the split flip disc mode; consequently, development of an analytical description of this plastic failure mechanism is the focus of this paper.

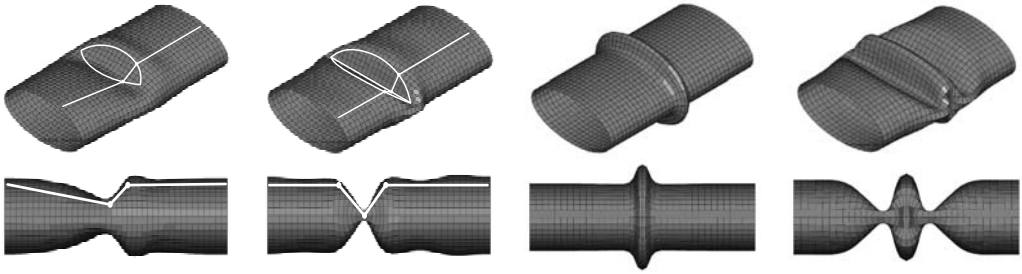

(a) Flip disc (b) Split flip disc (c) Elephant foot (d) Yoshimura

Figure 2. Plastic collapse mechanisms obtained from FE models for EHS.

5 ANALYTICAL MODELLING

In this section, an analytical model for the split flip disc failure mode arising in compressed EHS is developed based on the plastic theory for thin-walled structures presented by Murray [1]. As stated by Murray, assuming that the material stress-strain curve is a step function with a step height between tensile and compressive yielding of $2f_y$, where f_y is the material yield strength, a cross-section's load-carrying capacity can be derived as a function of the displacement from equilibrium, based on an assumed plastic collapse mechanism. Rigid-plastic material behaviour is therefore used, which neglects strain hardening, and assumes that all deformation is localised along the hinge lines with no deformation elsewhere.

The moment capacity of a plastic hinge, based on a rectangular element of width b and thickness t is:

$$M_{pl} = \frac{f_y b t^2}{4} \tag{2}$$

And the reduced plastic moment M'_{pl} in the presence of an axial load N may be shown to be:

$$M'_{pl} = M_{pl}\left(1 - \frac{N^2}{N_y^2}\right) \tag{3}$$

where N is the axial load and $N_y = f_y bt$ is the yield load in the element. Eq. 3 applies when the hinge line is perpendicular to the direction of the thrust. However, for an inclined hinge line, the reduced plastic moment is given by Eq. 4, where β is the angle between the line perpendicular to the thrust and the studied inclined hinge line.

$$M''_{pl} = M'_{pl} \sec^2 \beta \tag{4}$$

In the present work, both parabolic and elliptical functions were considered for the description of the curved hinge lines in the plastic mechanism. However, the parabolic hinge lines were found to more accurately replicate the actual load-displacement response of EHS, thus, this shape is used throughout the present derivation. A parabola can be defined using two parameters that fix the height X_h and the width S_h of the curve on the surface of the EHS. Hence, the values of X_h and S_h define the mechanism along the development of the plastic hinge (Eq. 5). Fig. 1 summarises the notation used in the present section to define the modelled failure mechanism, as well as the angle β used in Eq. 4.

$$x(s) = X_h\left(1 - \frac{s^2}{S_h^2}\right) \tag{5}$$

With reference to Fig. 1, the load transmitted by the complete cross-section can be obtained in terms of the load inside the plastic hinges (N_{in}) plus the load outside the plastic hinges (N_{out}). Furthermore, by using symmetry, only one quarter of the cross-section needs to be analysed with the result for the full cross-section being factored accordingly. The contribution to the load-carrying capacity of the cross-section from within the hinge lines and outside hinge lines are derived in the following two sub-sections.

5.1 Load-carrying contribution within the plastic hinges

Since the inclination of the hinge lines is variable around the cross-section, a differential strip of material is analysed, as depicted in Fig. 1, with the following reduced plastic moment:

$$M''_{pl} = \frac{f_y\ t^2}{4}\left(1 - \left(\frac{dN}{f_y\ t\ ds}\right)^2\right)\sec^2\beta\ dS \tag{6}$$

in which dN is the load in the strip and dS is the strip width. Fig. 3(a) presents the free body diagram of the material strip, that relates the lateral displacement of the strip Δ_{ds} to the applied load dN and the reduced plastic moment. The bending moment diagram in the material strip is presented in Fig. 3(b). The load borne by the strip dN can be related to the lateral displacement by considering equilibrium at a null bending moment point. For the split flip disc mechanism, the point of zero bending moment lies between the curved hinge line and the straight hinge line that splits the flip disc into two equal parts. Denoting Δ' the straight distance between the null bending moment point and the undeformed position (see Fig. 3(a)), this distance can be related to Δ_{dS} through the magnitudes of M'_{pl} and M''_{pl}, and consequently as a function of the plastic hinge inclination β:

$$\Delta' = \Delta_{dS}\frac{M''_{pl}}{M'_{pl} + M''_{pl}} = \Delta_{dS}\frac{\sec^2\beta}{1 + \sec^2\beta} \tag{7}$$

Figure 3. (a) Free body diagram and (b) bending moment diagram of the material strip.

Having obtained Δ', the load borne by the strip dN may be related to the reduced plastic moment:

$$dN\,\Delta' = M''_{pl} = M'_{pl}\sec^2\beta \tag{8}$$

Merging Eq. 7 and Eq. 8, introducing the reduced plastic moment in the material strip (Eq. 6) and rearranging, we obtain.

$$dN = f_y\ t\left(\sqrt{\left(\frac{2\Delta_{dS}}{(1+\sec^2\beta)\,t}\right)^2+1}-\frac{2\Delta_{dS}}{(1+\sec^2\beta)\,t}\right)dS \tag{9}$$

The lateral displacement in the strip Δ_{dS} can be related to the maximum lateral displacement in the hinge Δ through Eq. 10, where x(s) defines the parabolic shape of the curved hinge line (Eq. 5).

$$\Delta_{dS} = \Delta\frac{x(s)}{X_h} = \Delta\left(1-\frac{s^2}{S_h^2}\right) \tag{10}$$

From Eq. 9 and 10, and following some manipulation, we obtain the load carried by each strip as:

$$dN = f_y\ t\left(\sqrt{\left(\frac{S_h^2(S_h^2-s^2)\Delta}{(S_h^4+2X_h^2s^2)\,t}\right)^2+1}-\frac{S_h^2(S_h^2-s^2)\Delta}{(S_h^4+2X_h^2s^2)\,t}\right)dS \tag{11}$$

Eq. 11 can not be integrated explicitly; hence, in the present work Simpson's rule has been employed to obtain the load–lateral displacement curve, as advised in [1]. The load in the strip was evaluated at s = 0, s = S_h/2 and s = S_h, leading to the following relationship between load within the plastic hinges N_{in} (for one quarter of the section) and lateral displacement Δ for the split flip disc mechanism:

$$N_{in} = \frac{f_y\ t\ S_h}{6}\left(1-\frac{\Delta}{t}-\frac{6S_h^2\Delta}{(2S_h^2+X_h^2)\,t}+\sqrt{\frac{\Delta^2}{t^2}+1}+4\sqrt{\frac{9S_h^4\Delta^2}{4(2S_h^2+X_h^2)^2t^2}+1}\right) \tag{12}$$

5.2 Load-carrying contribution outside the plastic hinges

The area of the cross-section outside the plastic hinges is considered to be working at the yield stress. Hence, the load-carrying contribution from outside the plastic hinges is proportional to the arc length outside the hinge S_{out}, and is given for one quarter of the section as:

$$N_{out} = f_y\ t\,S_{out} \tag{13}$$

The total load carried by the full cross-section is obtained from Eq. 12 and Eq. 13 as:

$$N(\Delta) = 4\left(N_{out}+N_{in}\right) \tag{14}$$

5.3 Governing parameters

Since the load-carrying capacity of the section depends on the shape of the plastic mechanism, X_h and S_h must be defined as a function of Δ in order to determine the final load–lateral displacement curve. At this point, information obtained from the FE models and the tests has been used to monitor the value of both parameters throughout the deformation process. The height of the parabola X_h has been observed to remain almost constant during deformation; its value may therefore be defined simply as a function of the cross-section dimensions. However, the width of the parabola S_h, has been seen to increase as lateral displacement increases. Furthermore, the FE models showed that S_h is not directly proportional to the lateral displacement, but grows more rapidly at the beginning of the deformation process and tends towards a final value. Hence, both X_h and S_h have been defined by means of the cross-section dimensions in the present work, X_h being constant throughout the deformation and S_h being a function of Δ.

As stated in [3], the longitudinal wavelength for elastic buckling of CHS is a function of the radius r and the thickness t. Clearly the elastic buckling wavelength is influential in the definition of the size of the plastic collapse mechanism, particularly at the early stages of the deformation process. Hence, the measured values of X_h from the FE models and the experiments have been plotted against $(D_e t)^{0.5}$ in Fig. 4. The data may be seen to follow an approximately linear trend, and hence Eq. 15 was obtained by least squares regression, ensuring that the line passes through the origin, and used in the analytical model.

$$X_h = 1.22\sqrt{D_e t} \tag{15}$$

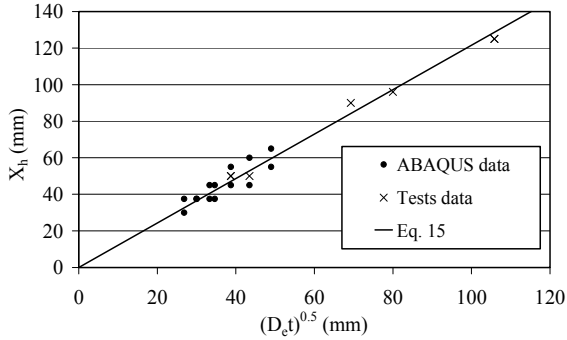

Figure 4. X_h values from the FE models and the tests.

The FE models showed that the S_h parameter increased more rapidly at the beginning of the plastic deformation than when the mechanism was fully developed. Hence, it was chosen to represent S_h with a rational expression of the form given by Eq. 16 that tends to $S_{h,a}$, and where C is a constant.

$$S_h = S_{h,a} \frac{\Delta}{\Delta + C} \tag{16}$$

Based on observations of the test failure patterns, it was found that the maximum extent of the plastic mechanism was approximately 75% of the way around the quarter perimeter of the section – i.e. $S_{h,a} = 0.75P/4 = 3P/16$, where P is the perimeter of the ellipse. Furthermore, from the FE results, it was found that C = t provided a good approximation of the progression of S_h towards its asymptotic value. Hence, Eq. 17 was established:

$$S_h = \frac{3P}{16}\left(\frac{\Delta}{\Delta + t}\right) \tag{17}$$

6 COMPARISON OF ANALYTICAL MODEL WITH OBSERVED BEHAVIOUR

The analytical equations developed throughout Section 5 are validated in this section by reference to the results of the FE study. Load-lateral displacement curves for two cases are shown in Fig. 5 – EHS 150×75×4 and EHS 150×75×8, representing the extremes of slenderness in currently available elliptical steel profiles. An initial geometric amplitude of t/100 was used in the FE models, since this had being found to provide the best agreement with test results [2]. The comparisons reveal good agreement between the results of the analytical model and of the FE simulation. For the sections investigated, a maximum deviation between the two load-lateral displacement curves of 6.7% was observed.

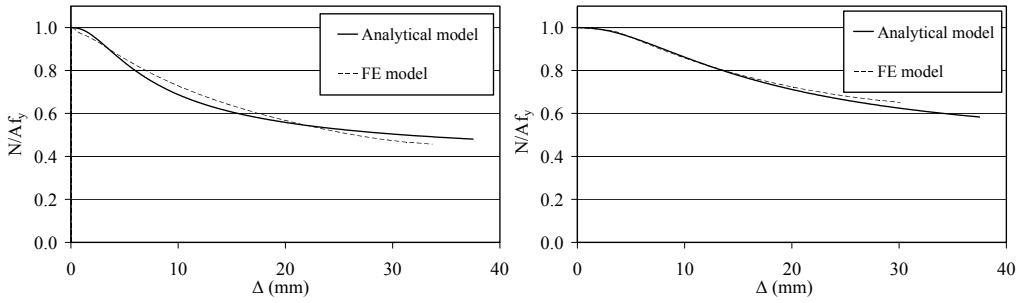

(a) t = 4 mm (b) t = 8 mm

Figure 5. Load-lateral displacement comparisons for 150×75 EHS with (a) t = 4 mm and (b) t = 8 mm.

7 CONCLUSIONS

Local plastic collapse mechanisms in compressed EHS have been examined in this study. Four collapse mechanisms were identified, two of which were akin to plate-like behaviour and two to shell-like behaviour. A numerical study, coupled with examination of existing test data, revealed that the so-called split flip disc mechanism arose most frequently. Hence an analytical model to describe the load–lateral displacement response of EHS under pure compression following this failure pattern was derived. Simple expressions, in terms of section geometry, to determine the key parameters required to fully describe the shape of the collapse mechanism were developed. Comparisons between the analytical model and FE model revealed good agreement over a range of cross-section slenderness, with a maximum discrepancy of 6.7%. It is concluded that the derived analytical model provides an accurate means of predicting the load-lateral displacement response of a compressed EHS undergoing local plastic collapse in the split flip disc mechanism.

ACKNOWLEDGEMENTS

The authors would like to acknowledge the Basque Government (Department of Education, Universities and Research) for the financial support given under the overseas post-doctoral development scheme in 2009 and 2010.

REFERENCES

[1] Murray NW. Introduction to the theory of thin-walled structures. Oxford University Press 1984. ISBN 0-19-856186-5.

[2] Chan TM and Gardner L. Compressive resistance of hot-rolled elliptical hollow sections. Engineering Structures 2008;30(2),522–532.

[3] Ruiz-Teran A and Gardner L. Elastic buckling of elliptical tubes. Thin-Walled Structures 2008;46(11):1304-1318.

[4] Andrews KRF, England GL and Ghani E. Classification of the axial collapse of cylindrical tubes under quasi-static loading. International Journal of Mechanics and Science 1983;25(9):687-696.

[5] Guillow SR, Lu G and Grzebieta RH. Quasi-static axial compression of thin-walled circular aluminium tubes. International Journal of Mechanical Sciences 2001;43(9):2103–2123.

[6] Grzebieta RH. An alternative method for determining the behaviour of round stocky tubes subjected to an axial crush load. Thin-Walled Structures 1990;9(1-4):61-89.

[7] Gupta NK and Velmurugan R. An analysis of axi-symmetric axial collapse of round tubes. Thin-Walled Structures 1995;22(4):261-274.

[8] Johnson W, Soden PD and Al-Hassani STS. Inextensional collapse of thin-walled tubes under axial compression. Journal of Strain Analysis 1977;12(4):317-330.

[9] Zhao XL and Packer JA 2009. Tests and design of concrete-filled elliptical hollow section stub columns. Thin-Walled Structures, 47(6-7): 617-628.

[10] Chan TM and Gardner L. Bending strength of hot-rolled elliptical hollow sections. Journal of Constructional Steel Research 2008;64(9):971-986.

[11] Gardner L and Chan TM. Cross-section classification of elliptical hollow sections. Steel and Composites Structures 2007;7(3):185-200.

[12] Kemper J. Some results on buckling and postbuckling of cylindrical shells. Collected papers on instability of shell structures. NASA TND-1510, Dec. 1962:173-186. Polytechnic Inst. Brooklyn.

[13] Silvestre N. Buckling behaviour of elliptical cylindrical shells and tubes under compression. International Journal of Solids and Structures 2008;45(16):4427-4447.